

# SPARSE TRAINING OF DISCRETE DIFFUSION MODELS FOR GRAPH GENERATION

Yiming Qin, Clément Vignac, Pascal Frossard \*

LTS4, EPFL, Lausanne, Switzerland

## ABSTRACT

Generative graph models struggle to scale due to the need to predict the existence or type of edges between all node pairs. To address the resulting quadratic complexity, existing scalable models often impose restrictive assumptions such as a cluster structure within graphs, thus limiting their applicability. To address this, we introduce SparseDiff, a novel diffusion model based on the observation that almost all large graphs are sparse. By selecting a subset of edges, SparseDiff effectively leverages sparse graph representations both during the noising process and within the denoising network, which ensures that space complexity scales linearly with the number of chosen edges. During inference, SparseDiff progressively fills the adjacency matrix with the selected subsets of edges, mirroring the training process. Our model demonstrates state-of-the-art performance across multiple metrics on both small and large datasets, confirming its effectiveness and robustness across varying graph sizes. It also ensures faster convergence, particularly on larger graphs, achieving a fourfold speedup on the large Ego dataset compared to dense models, thereby paving the way for broader applications. <sup>1</sup>

## 1 INTRODUCTION

Over the past decades, random graph models have played a foundational role in graph generation (Erdős et al., 1960; Barabási, 2013). However, recent advances in capturing complex data distributions have redirected research efforts towards learned graph models. In this domain, traditional frameworks such as generative adversarial networks (De Cao & Kipf, 2018) and variational autoencoders (Simonovsky & Komodakis, 2018), which were primarily focused on small graphs, have been succeeded by denoising diffusion models (Niu et al., 2020; Jo et al., 2022; Vignac et al., 2023a). These diffusion models not only set new benchmarks in various graph generation tasks but also partially addressed the scalability limitations, capable of generating graphs with up to 200 nodes. However, current diffusion models still struggle to scale to large graphs required for broader applications such as transportation (Rong et al., 2023) or anomaly detection in financial systems (Li et al., 2023).

The primary complexity constraint in graph generative models arises from the need to predict interactions for all node pairs, leading to quadratic computational complexity relative to the number of nodes. Methods to mitigate this limitation include imposing node ordering (Dai et al., 2020), assembling sub-graphs (Limnios et al., 2023), hierarchical generation (Karami, 2023; Jang et al., 2023; Bergmeister et al., 2023), and conditioning on a sampled degree distribution (Chen et al., 2023). While these approaches are designed for large graphs, they require additional assumptions such as cluster structures or dependencies on node degrees. Their suboptimal performance in applications like molecule generation (Chen et al., 2023; Kong et al., 2023) casts doubt on the robustness of these assumptions.

Motivated by the above limitations, and considering that real-world graphs are mostly sparse, we propose SparseDiff, a discrete diffusion model that only harnesses the inherent sparsity of training graphs without imposing extra assumptions, enabling more general application to diverse downstream tasks. Specifically, SparseDiff employs a sparse representation based on edge lists to address

\*Contact: first\_name.last\_name@epfl.ch

<sup>1</sup>Our code is available at <https://github.com/qym7/SparseDiff>.

the quadratic space complexity inherent in three key components of a diffusion model. It introduces: 1) A computationally efficient noise model that maintains the sparsity of noisy graphs, 2) A sparse denoising network trained on a random subset of node pairs, 3) An iterative sampling procedure designed to progressively populate the dense adjacency matrix with sparse inputs. Each component maintains linear complexity with respect to the number of edges while enabling it to handle graphs of varying sizes effectively. By specifying the size of the subset of edges used, SparseDiff ensures controllable space complexity during both the training and inference phases. Our work represents the first application of sparse representations for graph diffusion, significantly differentiating itself from previous methods based on hierarchical or autoregressive frameworks.

Our experiments demonstrate that SparseDiff not only achieves state-of-the-art performance but also converges significantly faster than dense diffusion models on large graphs such as protein interaction networks (Protein) and social networks (Ego). Remarkably, it also outperforms dense models like SPECTRE (Martinkus et al., 2022) and DiGress (Vignac et al., 2023a), as well as other scalable models like EDGE (Chen et al., 2023) and HGGT (Jang et al., 2023), in managing smaller molecular datasets like QM9 and Moses. These results empirically validate the effectiveness of our sparse modeling approach and confirm its robustness across a diverse range of datasets without relying on additional assumptions.

## 2 RELATED WORK

### 2.1 DENOISING DIFFUSION MODELS FOR GRAPHS

Diffusion models have gained increasing popularity due to their impressive performance across various generative tasks in fields such as computer vision (Dhariwal & Nichol, 2021; Ho et al., 2022), protein generation (Baek et al., 2021; Ingraham et al., 2022), and audio synthesis (Kong et al., 2020). These models are characterized by three core components. The first is a Markovian noise model, which progressively corrupts a data point  $x$  to a noisy sample  $z^t$  over iterative steps  $t$  from 1 to  $T$ , until it conforms to a predefined prior distribution at step  $T$ . The second component is a denoising network, parametrized by  $\theta$ , which is trained to restore the corrupted data back to its less noisy state. Typically, this network aims to predict the original data  $x$  given the noisy sample  $x_t$ . The third component is the reverse process for data generation, where a fully noisy data point  $z^T$  is first sampled from a prior distribution. The denoising network then operates at each time step  $t \in [T, \dots, 1]$  to predict the less noisy distribution according to  $p_\theta(z^{t-1}|z^t) = \int_x q(z^{t-1}|z^t, x) dp_\theta(x|z^t)$ , from which a new data point  $z^{t-1}$  is sampled. While this integral is generally difficult to evaluate, two prominent frameworks, Gaussian diffusion (Ho et al., 2020) and discrete diffusion (Austin et al., 2021), facilitate its efficient computation.

Initial graph diffusion models employed Gaussian noise directly on adjacency matrices (Niu et al., 2020; Jo et al., 2022). These models use a graph attention network to regress the added noise  $\epsilon$ , where  $\epsilon = z^t - z$ , effectively regressing the noise up to an affine transformation, akin to regressing the discrete clean graph. To preserve the inherent discreteness of graphical data, subsequent models (Vignac et al., 2023a; Haefeli et al., 2022) have leveraged discrete diffusion, reformulating graph generation as a series of classification tasks, and achieving top-tier results. However, these models require predictions for all pairs of nodes, which implies a quadratic space complexity and thus restricts their scalability.

### 2.2 SCALABLE GRAPH GENERATION

Efforts to enhance the scalability of graph generative models mainly follow two paradigms: hierarchical refinement and subgraph aggregation. The hierarchical refinement approach initially generates a low-resolution graph, which undergoes successive refinements for enhanced detail (Yang et al., 2021; Karami, 2023). For instance, the HGGT model (Jang et al., 2023) employs a hierarchical  $K^2$ -tree representation. For molecule generation, fragment-based models (Jin et al., 2018; 2020; Maziarz et al., 2022) adeptly assemble compounds using pre-defined molecular fragments. Recently, Bergmeister et al. (2023) proposes a hierarchical diffusion model based on spectrum-preserving local expansion algorithms, enabling the generation of non-attributed large graphs. On the other side, the subgraph aggregation approach divides larger graphs into smaller subgraphs, which are subsequently combined. For instance, SnapButton (Yang et al., 2021) enhances autore-

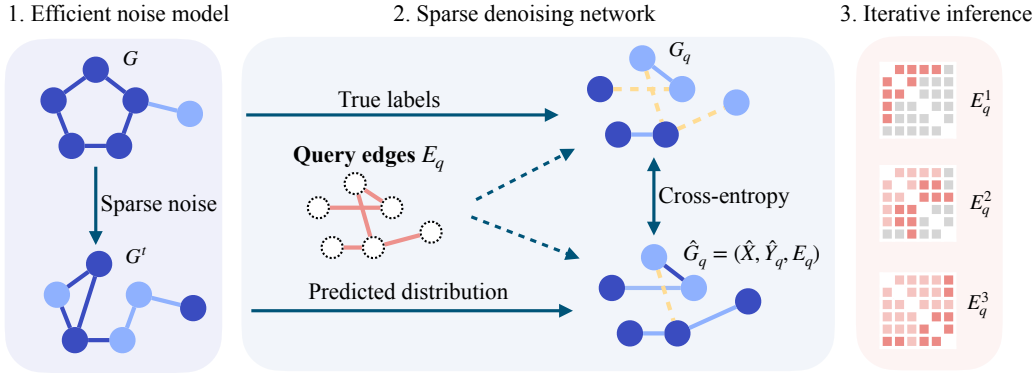


Figure 1: SparseDiff has three main components. First, to define the diffusion process, it constructs a sparse noise model that samples noise trajectories with linear space complexity relative to the number of edges. During network training, rather than considering all node pairs, SparseDiff randomly selects a subset of "query edges" ( $E_q$ ) based on a sparsity parameter  $\lambda$ , set to  $\frac{1}{3}$  for this visualization.  $E_q$  includes both 'existing' edges from the original graph and 'non-existing' edges, which will potentially become new edges, enabling the model to learn all edge types while efficiently managing space complexity. In the inference phase, SparseDiff predicts labels only for the query edges  $E_q^i$  in each iteration  $i$ , ensuring consistency with the training phase.

gressive models (Liu et al., 2018; Liao et al., 2019; Mercado et al., 2021) by merging subgraphs, and SaGess (Limnios et al., 2023) trains a dense diffusion model to generate subgraphs sampled from a large graph that are then merged.

Additionally, some approaches predict all node pairs in an auto-regressive way. Kong et al. (2023) integrated diffusion with autoregressive models, suggesting learning the node ordering, which is theoretically as difficult as isomorphism testing. On the other hand, EDGE (Chen et al., 2023) uses absorbing states to create sparse diffusion. It starts by generating a node degree distribution  $d^0$  and gradually constructs an adjacency matrix  $A$  based on the changes of node degrees during inference. While this factorization is universally applicable, the feasibility of learning the conditional distribution  $p_\theta(A|d^0)$  remains uncertain, as not all degree distributions can be achieved by undirected graphs.

Overall, scalable generation models typically either introduce a dependence on node orderings or rely heavily on extra assumptions on data distribution. In contrast, the SparseDiff model described in the next section aims at making no assumption besides graph sparsity, while showing competitive performance compared to other scalable models across a wide range of graphs.

### 3 SPARSEDIFF: SPARSE DISCRETE DIFFUSION FOR GRAPH GENERATION

We now introduce SparseDiff, a Sparse Denoising Diffusion Model designed to enhance the scalability of graph diffusion and extend the reach of discrete graph models to graphs with up to 1,000 nodes, a significant improvement over previous dense models limited to around 200 nodes.

Unlike previous graph diffusion models, SparseDiff builds on a sparse representation of graphs. A graph  $G$ , consisting of  $n$  nodes and  $m$  edges, is represented as a triplet  $(E, X, Y)$ . Here,  $E \in \mathbb{N}^{2 \times m}$  indicates the edge list with the indices of endpoints. Node and edge attributes are considered to be discrete and are encoded in a one-hot format as  $X \in \{0, 1\}^{n \times a}$  and  $Y \in \{0, 1\}^{m \times b}$ , where  $a$  and  $b$  are the number of classes, respectively. In particular, 'non-existing' edges are considered an additional edge type, while edges in  $E$  are referred to as 'existing' edges. This sparse representation is widely supported by standard graph processing packages such as Pytorch Geometric (Fey & Lenssen, 2019).

This work focuses solely on undirected graphs with discrete attributes, although continuous labels can be seamlessly integrated, as demonstrated by Vignac et al. (2023b). All considered graphs are free of self-loops. Figure 1 provides an overview of the SparseDiff framework. Further details on the

training and sampling processes are provided in Algorithms 1 and 2, respectively. In the following parts, we specifically focus on three critical components of the proposed sparse diffusion model for graphs: the noise model, the denoising network, and the iterative sampling algorithm.

### 3.1 EFFICIENT NOISE MODEL

To improve memory efficiency, SparseDiff employs a dedicated noise model that maintains a similar sparsity level of the noisy graph  $G^t$  throughout the noising process. This model also reduces the space complexity of computing noisy graphs from  $O(n^2)$  to  $O(m)$ .

#### 3.1.1 SPARSE TRAJECTORY

Given that Gaussian noise applied to the adjacency matrix typically results in dense noisy graphs, where all edge entries acquire continuous values (Niu et al., 2020; Jo et al., 2022)—we opt for a discrete diffusion framework. In this framework, we only need to consider the existing edges within a noisy graph, thereby reducing the number of edges necessary for computation.

In the discrete graph diffusion model, the noisy trajectory at each step is defined by  $q(G^t|G^{t-1}) = (\mathbf{X}\mathbf{Q}_X^t, \mathbf{Y}\mathbf{Q}_Y^t)$ , where  $\mathbf{Q}^t$  denotes the Markov transition matrix for that step, which transforms  $G^{t-1}$  into a noisier distribution. Various types of Markov transition matrices are employed, including uniform, absorbing (Austin et al., 2021), and marginal transitions (Vignac et al., 2023a). We employ the marginal transition model, which favors transitions towards the dominant class in the marginal distribution. This strategy is particularly effective for preserving sparse trajectories in graphs by naturally biasing the model toward ‘non-existing’ edges. Formally, considering the marginal distribution vectors  $\mathbf{p}_X$  for node types and  $\mathbf{p}_E$  for edge types, and denoting their transposes by  $\mathbf{p}'$ , the noise level at each step  $t$  is regulated by  $\beta^t$ , with  $\alpha^t = 1 - \beta^t$ . The marginal transition matrices are defined as follows:

$$\mathbf{Q}_X^t = \alpha^t \mathbf{I} + \beta^t \mathbf{1}_a \mathbf{p}'_X, \quad \mathbf{Q}_Y^t = \alpha^t \mathbf{I} + \beta^t \mathbf{1}_b \mathbf{p}'_Y.$$

Here,  $\mathbf{1}_a$  and  $\mathbf{1}_b$  are column vectors of ones with dimensions equal to the number of classes  $a$  for nodes and  $b$  for edges. These matrices incorporate a first term, the identity matrix  $\mathbf{I}$ , to preserve the distribution from  $G^{t-1}$ , and a second term to introduce noise aligned with the marginal distributions.

By employing continuous multiplication, we can derive the distribution at step  $t$  directly from the initial clean graph using  $q(G^t|G) = (\mathbf{X}\bar{\mathbf{Q}}_X^t, \mathbf{Y}\bar{\mathbf{Q}}_Y^t)$ , facilitating an immediate transition to the noisy state without the need for iterative step-by-step calculations. For instance, the cumulative transition matrix  $\bar{\mathbf{Q}}^t$  for nodes  $\mathbf{X}$  is as follows:  $\bar{\mathbf{Q}}_X^t = \mathbf{Q}_X^1 \mathbf{Q}_X^2 \dots \mathbf{Q}_X^t = \bar{\alpha}^t \mathbf{I} + (1 - \bar{\alpha}^t) \mathbf{1}_a \mathbf{p}'_X$ , where  $\bar{\alpha}^t = \alpha^1 \alpha^2 \dots \alpha^t$ . The parameter  $\bar{\alpha}^t$  starts very close to 1 at  $\bar{\alpha}^1$  and approaches 0 by  $\bar{\alpha}^T$ , reflecting a gradual increase in noise influence over diffusion process.

We note that this choice of marginal noise model does not guarantee that the noisy graph is always sparse. However, it is the case with high probability, as stated by the following lemma, which is an application of Desolneux et al. (2008) (detailed in Appendix A).

**Lemma 3.1.** (*Probability Bound for Sparsity in Noisy Graphs*) Consider an undirected graph with  $n$  nodes,  $m$  edges, and no self-loops. If the edge ratio given by  $m / \binom{n(n-1)}{2}$  is denoted as  $r$ , and the edge ratio in the noisy graph sampled from the marginal transition noise model is given by  $r_t$ , then for  $n$  sufficiently large and  $r < \frac{1}{4}$ , for any  $r < k < 1$ , we have:

$$\log(\mathbb{P}[r_t \geq k]) \sim -\frac{n(n-1)}{2} \left( k \log \frac{k}{r} + (1-r) \log \frac{1-k}{1-r} \right) \quad (1)$$

This lemma shows that, in large and sparse graphs, the probability of the edge ratio  $r_t$  in the noisy graph exceeding  $k$ , where  $k > r$ , declines exponentially with the graph size. As an example, for  $r$  small and  $k = 2r$ , this probability is approximated by  $c_1 e^{-c_2 n^2 r}$ , where  $c_1$  and  $c_2$  are constants. This probability diminishes significantly as the graph size  $n$  increases.

#### 3.1.2 SPARSE COMPUTATION

Our second requirement for the noise model is subquadratic space complexity sampling. Standard discrete diffusion models encode all edges using  $\mathbf{Y} \in \mathbb{R}^{n \times n \times b}$  and calculate transition probabilities

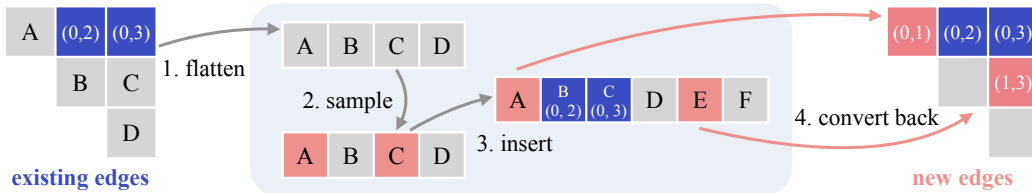


Figure 2: Efficient sampling of new edge positions among ‘non-existing’ positions using only the edge list, thus avoiding the quadratic space complexity of an adjacency matrix. The process involves: 1) **Flattening** the pair representations into a linear array, 2) **Sampling** uniformly from four non-occupied positions, selecting A (1<sup>st</sup>) and C (3<sup>rd</sup>), 3) **Inserting** offsets of 0 and 2 to the positions of A and C to account for the count of ‘existing’ edges before the selected positions, resulting in positions A (1<sup>st</sup>) and E (5<sup>th</sup>), 4) **Converting** these positions back to index pairs (0, 1) and (1, 3).

with  $Y\bar{Q}_Y^t \in \mathbb{R}^{n \times n \times b}$ , which incurs  $O(n^2)$  space complexity. To facilitate sparse sampling, we differentiate between ‘existing’ and ‘non-existing’ edges. In sparse graphs, where ‘existing’ edges are a minority, we compute  $YQ_Y^t \in \mathbb{R}^{m \times b}$  for these edges and sample their new labels from this distribution. Edges transitioning to ‘non-existing’ are then removed to preserve sparsity in  $G^t$ . Conversely, for the majority ‘non-existing’ edges in sparse graphs, we use a novel three-step approach to sample without using dense adjacency matrices. The process involves:

1. Sampling the number of new ‘existing’ edges.
2. Sampling positions for new edges uniformly from non-occupied node pairs (c.f. Fig. 2).
3. Sampling the edge attributes from all labels except ‘non-existing’.

Specifically, the number of new edges, that is, ‘non-existing’ edges transitioning to ‘existing’, follows a Binomial distribution  $\mathcal{B}(\bar{m}_t, q_t)$ . Here,  $\bar{m}_t = \frac{n(n-1)}{2} - m_t$  represents the total possible edges minus the ‘existing’ ones in  $G^t$ . With ‘non-existing’ as the first class,  $q_t = 1 - Q^t[0, 0]$  indicates the transition probability from ‘non-existing’ to ‘existing’ edge types. New edge labels are determined by a Multinomial distribution as specified by  $Q^t[0, 1 : ]$ . This method markedly improves efficiency and scalability in modeling large graphs.

The second step, sampling new edge positions, presents more challenges. As illustrated in Figure 2, our algorithm efficiently handles the sparse sampling without requiring a full adjacency matrix. The method begins by flattening the graph’s vacant position pair representations into a linear array. We then perform simple random sampling from this array and then adjust the sampled indices by adding offsets to accommodate existing edges, before remapping them to index pairs. This process accommodates simultaneous sampling across batches of graphs with varying sizes, ensuring efficient space usage and precise placement of new edges.

### 3.2 EFFICIENT DENOISING NEURAL NETWORK

Unlike traditional graph diffusion models that encode features for every node pair with a computational complexity of  $O(ln^2d_e)$ , where  $l$  represents the layer count and  $d_e$  the dimension of edge activations, our approach builds on a memory-efficient graph neural network that utilizes edge lists, significantly reducing the complexity to  $O(lmd_e)$ , where  $m$  is the number of chosen edges involved in message-passing. This efficiency is achieved by leveraging sparse representations within message-passing neural networks (MPNNs) (Scarselli et al., 2008; Gilmer et al., 2017), utilizing specialized libraries like Pytorch Geometric (Fey & Lenssen, 2019) or the Deep Graph Library (Wang, 2019).

Specifically, our architecture differs from most message-passing networks by needing to make predictions for all node pairs instead of ‘existing’ ones. This shift explains why previous models employed graph transformer networks (Vignac et al., 2023a), which inherently encode each node pair within their full attention layers. To circumvent this need, a common strategy for knowledge graphs (Zhang & Chen, 2018; Chamberlain et al., 2022; Boschini, 2023) involves predicting edge labels based on the pairwise similarity between node embeddings. Although theoretically feasible, this

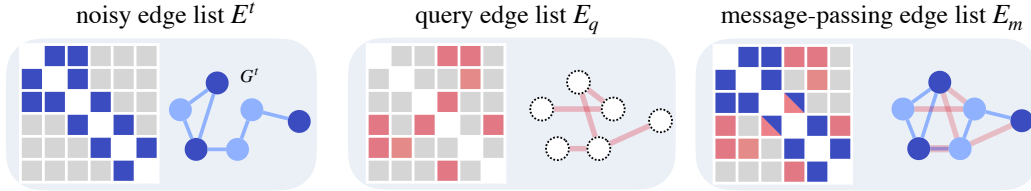


Figure 3: The message-passing edge list  $E_m$ , fed to the sparse denoising network, comprises noisy edges  $E^t$  (shown in blue) and uniformly sampled query edges  $E_q$  (shown in red).

link-prediction method fails to reach the performance of dense denoising models (detailed in Table 13 in Appendix D.6), even on small graph datasets. Consequently, edges for prediction have to be explicitly encoded to enhance prediction accuracy in practice.

### 3.2.1 EDGE PREDICTION MODULE

As previously discussed, relying solely on node features for edge prediction yields limited results. To enhance edge prediction, we randomly select a subset of node pairs for explicit encoding during each forward pass, termed ‘query edges’. As indicated in Figure 3, the input to the denoising network, referred to as message-passing edges  $(E_m, Y_m)$ , thus includes two sets of edges: ‘noisy edges’  $(E^t, Y^t)$ , representing ‘existing’ edges in the noisy graph  $G^t$ , and ‘query edges’  $(E_q, Y_q)$ , which are random edges selected for prediction. Noisy edges preserve the topological information of the noisy graph, while query edges, sampled randomly from all node pairs, include both ‘existing’ and ‘non-existing’ edges, enabling the model to predict all edge types. To provide an unbiased estimator of the loss relative to dense diffusion models, query edges are uniformly sampled across each graph.

Additionally, the ‘non-existing’ edges included in  $E_q$  serve as shortcuts within the message-passing network, a mechanism that facilitates graph rewiring. This is known to enhance information propagation and mitigate over-squashing issues, as noted in studies like (Alon & Yahav, 2020; Topping et al., 2021; Di Giovanni et al., 2023).

To control the number of query edges, we define the ‘sparsity parameter’  $\lambda$  as the ratio of query edges to all node pairs. Given that query edges may overlap with noisy edges and the number of noisy edges  $m_t$  approximates the number of edges  $m$  in the clean graph according to Lemma 3.1, the total number of message-passing edges is approximately upper bounded by  $(m + \lambda n^2)$ . By setting  $\lambda = \frac{m}{n^2}$ , the computational complexity of SparseDiff practically aligns linearly with the number of edges  $m$  in the clean graph  $G$ . In our experiments,  $\lambda$  is chosen to enable an effective batch size for training, as detailed in Appendix C.2. This parameter provides flexibility under varying computational conditions.

### 3.2.2 MODEL TRAINING

Our sparse denoising network adopts a graph transformer architecture featuring normalization, feed-forward, and attention layers (Veličković et al., 2017). It incorporates a sparse attention mechanism for handling sparse data (Shi et al., 2020), and integrates advanced features such as PNA pooling layers (Corso et al., 2020) and FiLM layers (Perez et al., 2018), which are designed to enhance predictive accuracy and effectively manage computational complexity. A detailed discussion of the model architecture is provided in Appendix B.

Training of the network involves predicting ‘query edges’  $E_q$ , and the loss is minimized using the cross-entropy (CE) loss between the predicted distribution  $\hat{P}_q^G = (\hat{P}_q^X, \hat{P}_q^Y)$  and the clean graph  $G$ . The loss function is computed as follows:

$$\sum_{1 \leq i \leq n} \text{CE}(\mathbf{X}_i, \hat{P}_i^X) + \frac{c}{\lambda} \sum_{(i,j) \in E_q} \text{CE}(\mathbf{Y}_{ij}, \hat{P}_{ij}^Y), \quad (2)$$

Here, the constant  $c$  weights nodes and edges in the loss calculation. It is rescaled by dividing by  $\lambda$  to maintain a consistent edge-to-node weight ratio across different  $\lambda$  values.

**Algorithm 1** Sparse training at step  $t$  with the sparsity parameter  $\lambda$  (Section 3.1 & 3.2)

- 
- 1: Given the clean graph  $G = (\mathbf{E}^0, \mathbf{X}^0, \mathbf{Y}^0)$ ;
  - 2: Sample the noisy graph  $G^t = (\mathbf{E}^t, \mathbf{X}^t, \mathbf{Y}^t)$ ;
  - 3: Sample query edges  $\mathbf{E}_q$  of size  $\lceil \lambda n^2 \rceil$  ;
  - 4:  $\mathbf{E}_m \leftarrow \mathbf{E}^t \cup \mathbf{E}_q, \mathbf{Y}_m \leftarrow \mathbf{Y}^t \cup \mathbf{Y}_q$ ; ▷ Construct message-passing edges
  - 5:  $G_m \leftarrow (\mathbf{E}_m, \mathbf{X}^t, \mathbf{Y}_m)$ ; ▷ Construct the message-passing graph
  - 6:  $(\hat{\mathbf{P}}^{\mathbf{X}}, \hat{\mathbf{P}}^{\mathbf{Y}}) = \phi_\theta(G_m, \mathbf{E}_q)$ ; ▷ Predict the distribution of nodes and query edges
  - 7: optimizer.step(CE( $\hat{\mathbf{X}}^0, \hat{\mathbf{P}}^{\mathbf{X}}$ ) + CE( $\mathbf{Y}_q^0, \hat{\mathbf{P}}^{\mathbf{Y}}$ )); ▷ Loss calculation
- 

**Algorithm 2** Iterative inference at step  $t$  with the sparsity parameter  $\lambda$  (Section 3.3)

- 
- 1: Initialize an empty graph  $G^{t-1}$  with unlabeled nodes  $\mathbf{X}^{t-1}$  and no edges;
  - 2: Randomly divide all node pairs into  $K = \lceil \frac{1}{\lambda} \rceil$  equal-sized chunks  $\{C_0, \dots, C_{K-1}\}$ ;
  - 3: **for**  $k$  in range( $K$ ) **do**
  - 4:  $\mathbf{E}_q \leftarrow C_k$ ; ▷ Set query edges
  - 5:  $\mathbf{E}_m \leftarrow \mathbf{E}^t \cup \mathbf{E}_q$ ; ▷ Construct message-passing edges and its attributes  $\mathbf{Y}_m$
  - 6:  $G_m \leftarrow (\mathbf{E}_m, \mathbf{X}^t, \mathbf{Y}_m)$ ; ▷ Construct the message-passing graph
  - 7:  $(\hat{\mathbf{P}}^{\mathbf{X}}, \hat{\mathbf{P}}^{\mathbf{Y}}) = \phi_\theta(G_m, \mathbf{E}_q)$ ; ▷ Predict the distribution of nodes and query edges
  - 8:  $\hat{\mathbf{X}} = \text{Multinomial}(\hat{\mathbf{P}}^{\mathbf{X}}), \hat{\mathbf{Y}}_q = \text{Multinomial}(\hat{\mathbf{P}}^{\mathbf{Y}})$ ; ▷ Sample labels
  - 9:  $\mathbf{X}^{t-1} \leftarrow \hat{\mathbf{X}}$ ; ▷ Assign node new labels
  - 10:  $\mathbf{Y}^{t-1} \leftarrow \mathbf{Y}^{t-1} \cup \hat{\mathbf{Y}}_q[\hat{\mathbf{Y}}_q! = 0], \mathbf{E}^{t-1} \leftarrow \mathbf{E}^{t-1} \cup \hat{\mathbf{E}}_q[\hat{\mathbf{Y}}_q! = 0]$ ; ▷ Add ‘existing’ edges
- 

## 3.3 ITERATIVE INFERENCE

SparseDiff also remains memory-efficient at the inference stage. Here, we first sample the number of nodes  $n$  from the node distribution of the training set, which remains constant during the reverse process. Next, we sample a random graph from the prior distribution  $G^T \sim \prod_{i=1}^n \text{Cate}(\mathbf{p}_{\mathbf{X}}) \times \prod_{1 \leq i < j \leq n} \text{Cate}(\mathbf{p}_{\mathbf{Y}})$ , where  $\mathbf{p}_{\mathbf{X}}$  and  $\mathbf{p}_{\mathbf{Y}}$  represent the marginal probabilities of node and edge classes, respectively. The categorical distribution  $\text{Cate}(\mathbf{p})$  is used for both nodes and edges. The sparse denoising network  $\phi_\theta$  is then recursively applied to predict the clean graph from the noisy one. The generation process of SparseDiff is visualized in Figure 6.

Directly predicting the entire graph at each diffusion step  $t$  is impractical due to quadratic memory requirements. Moreover, using dense graphs during inference could lead to a distribution shift caused by changes in the number of edges used for message-passing. To mitigate this, we implement an iterative procedure to progressively cover all node pairs in  $G^{t-1}$ . As detailed in Algorithm 2, we divide all node pairs randomly into  $K = \lceil \frac{1}{\lambda} \rceil$  equally-sized sets, representing the query edges for each prediction step<sup>2</sup>. During each iteration  $k$ , the noisy graph  $G^t$  remains identical, and a message-passing edge list  $\mathbf{E}_m$  is constructed using noisy edges and query edges from the  $k^{\text{th}}$  set. SparseDiff then predicts the distributions for these query edges, samples labels, and integrates edges classified as ‘existing’ into  $G^{t-1}$ .

This iterative approach allows SparseDiff to maintain favorable memory complexity, albeit at the cost of increased sampling time due to iterations at each diffusion step. However, unlike many scalable models, SparseDiff does not impose additional assumptions about data distribution, such as clustering or degree distribution. Despite the increased sampling time, the generation time for SparseDiff remains efficient due to its ability to utilize larger batch sizes and to accelerate model computations using sparse inputs, as reported in Table 11 of Appendix D.4.

Besides, drawing inspiration from D3PM (Austin et al., 2021) and DDIM (Song et al., 2020), we propose a method to accelerate inference by reducing the inference steps by a factor  $k$ . In particular,

<sup>2</sup>When  $\frac{n(n-1)}{2}$  is not divisible by  $K$ , we adjust by slightly overlapping the last set with the previous one.

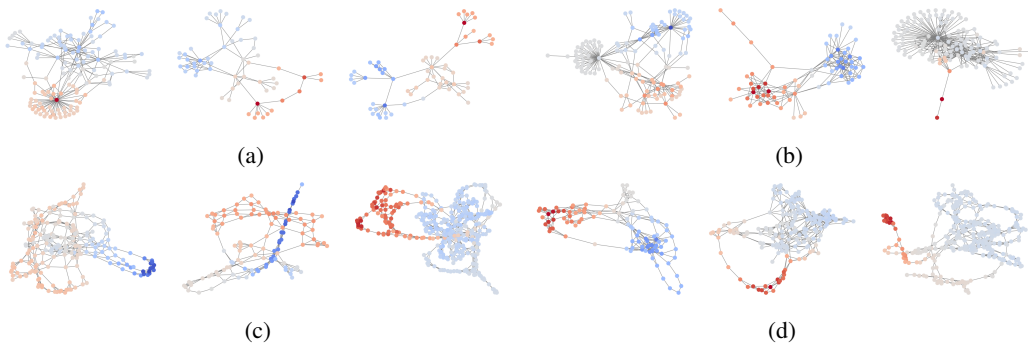


Figure 4: Samples from SparseDiff trained on large graphs. (a) Ego training set (50 to 399 nodes); (b) Generated Ego graphs; (c) Protein training set (100 to 500 nodes); (d) Generated Protein graphs.

at each step  $t$ , the model predicts  $q(G^{t-k}|G^t, G) \propto G^t(Q^t)' \odot G\bar{Q}^{t-k}$  instead of  $q(G^{t-1}|G^t, G) \propto G^t(Q^t)' \odot G\bar{Q}^{t-1}$ . The results for acceleration are reported in Table 5.

## 4 EXPERIMENTS

We conducted comprehensive experiments to evaluate the performance of SparseDiff across a diverse set of graphs comparing against a comprehensive range of models. These include GraphRNN (You et al., 2018), GRAN (Liao et al., 2019), GraphNVP (Madhawa et al., 2019), SPECTRE (Martinkus et al., 2022), GDSS (Jo et al., 2022), DiGress (Vignac et al., 2023a), DruM (Jo et al., 2023), and several scalable models such as BiGG (Dai et al., 2020), GraphARM (Kong et al., 2023), EDGE (Chen et al., 2023), HiGen (Karami, 2023), and HGGT (Jang et al., 2023). For clarity, we refer to the local expansion method proposed by Bergmeister et al. (2023) as GraphLE.

To ensure reliability, SparseDiff’s performance metrics are presented in the format of mean  $\pm$  standard deviation, based on five samplings. This accounts for the instability caused by limited test set sizes in some datasets, namely SBM and Planar datasets. We bold SparseDiff’s results if the best results fall within our method’s variance range, indicating that with an optimal seed, SparseDiff can achieve the best performance. The results highlight SparseDiff’s strong competitive advantage on datasets containing larger graphs, such as Planar, SBM, Protein, and Ego, as well as its state-of-the-art performance on datasets with small molecules, including QM9 and Moses (as detailed in Appendix D.3). Notably, SparseDiff is the only model thus far that exhibits competitive performance across both large and small graphs, and in both scenarios of attributed and unattributed graphs.

### 4.1 LARGE GRAPH GENERATION

**Dataset** We evaluate SparseDiff on diverse graph datasets to demonstrate its scalability and versatility. First, we test its ability to generate edge-crossing-free planar graphs with 64 nodes. Next, we assess its capacity to generate graphs with 2 to 5 communities using Stochastic Block Model (SBM) graphs, scaling up to 200 nodes—the largest size seen in models like DiGress (Vignac et al., 2023a). We also evaluate Ego and Protein datasets, with graphs up to 500 nodes, representing citation relationships and amino acid interactions within 6 Angstroms. The largest edge ratio for these datasets is 8.8%, confirming their sparsity. Detailed dataset statistics are in Appendix C.2. To further highlight our model’s scalability, we include the generation of a large graph with 1,045 nodes in Appendix D.1.

**Metrics** For evaluation, we use maximum mean discrepancy (MMD) metrics, standard in graph generation tasks. We report the validity of SBM graphs as the fraction passing a stochastic block model test, and for Planar graphs, the fraction that are planar and connected. For larger datasets, we also use the Radial Basis Function (RBF) MMD metric to assess fidelity and diversity using a randomly parametrized GNN (Thompson et al., 2022). Since MMD metrics often yield small values that are difficult to compare directly, we report Degree, Cluster, Orbit, Spectre and RBF MMD metrics in units of  $10^{-3}$ ,  $10^{-2}$ ,  $10^{-2}$ ,  $10^{-3}$  and  $10^{-2}$ , respectively. The theoretical optimal metrics,

Table 1: Sample quality on large graphs. The mean ratios to the reference of the Degree, Cluster, Orbit, and Spectre MMD metrics are reported to enable a comprehensive comparison.

Class	Model	Degree( $10^{-3}$ ) $\downarrow$	Cluster ( $10^{-2}$ ) $\downarrow$	Orbit ( $10^{-2}$ ) $\downarrow$	Spectre ( $10^{-3}$ ) $\downarrow$	Ratio $\downarrow$	RBF ( $10^{-2}$ ) $\downarrow$
<i>Protein</i>	<i>Reference</i>	0.3	0.7	0.3	0.5	1.0	1.4
	Dense	GRAN	2.0	4.9	13	5.1	17
Sparse	DiGress	5.9 $\pm$ 0.1	10 $\pm$ 1.4	5.1 $\pm$ 1.8	2.9 $\pm$ 0.5	14 $\pm$ 2.3	7.1 $\pm$ 1.5
	DRuM	1.9	6.6	3.5	3.0	8.4	–
	BiGG	1.0	2.6	2.3	4.5	5.9	–
	HiGen	1.2	4.4	2.3	2.5	5.7	–
	GraphLE	3.0	3.1	0.5	1.3	4.7	–
	SparseDiff	1.5 $\pm$ 0.3	3.4 $\pm$ 0.3	0.5 $\pm$ 0.8	1.4 $\pm$ 0.2	3.6 $\pm$ 1.1	3.8 $\pm$ 0.7
<i>Ego</i>	<i>Reference</i>	0.2	0.7	0.7	1.0	1.0	0.9
	Dense	DiGress	8.9 $\pm$ 1.6	5.4 $\pm$ 0.4	3.0 $\pm$ 0.3	19 $\pm$ 3.2	19 $\pm$ 3.1
Sparse	EDGE	58	18	5.2	–	107	6.6
	HiGen	47	0.3	3.9	–	81	4.5
	SparseDiff	3.7 $\pm$ 0.4	3.2 $\pm$ 0.1	2.0 $\pm$ 0.4	5.6 $\pm$ 0.8	7.9 $\pm$ 0.9	2.6 $\pm$ 0.3

Table 2: Sample quality on synthetic graphs. The mean ratios to the reference of the Degree, Cluster and Orbit MMD metrics are reported to enable a comprehensive comparison.

Dataset	Stochastic block model					Planar				
	Model	Degree $\downarrow$	Cluster $\downarrow$	Orbit $\downarrow$	Ratio $\downarrow$	V.U.N. $\uparrow$	Degree $\downarrow$	Cluster $\downarrow$	Orbit $\downarrow$	Ratio $\downarrow$
<i>Reference</i>	0.9	3.3	2.6	1.0	100%	0.2	3.1	0.1	1.0	100%
GRAN	5.5	5.8	7.9	3.6	25%	0.7	4.3	0.1	2.0	0%
GG-GAN	3.5	7.0	5.9	2.8	25%	63	118	123	528	0%
SPECTRE	1.5	5.2	4.1	1.6	53%	0.5	7.9	0.1	2.0	25%
DiGress	1.7 $\pm$ 0.1	5.0 $\pm$ 0.1	3.6 $\pm$ 0.4	1.6 $\pm$ 0.1	74% $\pm$ 4	0.8 $\pm$ 0.0	4.1 $\pm$ 0.3	0.5 $\pm$ 0.0	1.2 $\pm$ 0.4	76% $\pm$ 1
DruM	0.7	4.9	4.5	3.6	85%	0.5	3.5	0.1	1.5	90%
HiGen	5.5	5.8	7.9	3.6	–	–	–	–	–	–
GraphLE	12	5.2	6.7	5.8	45%	0.5	6.3	0.2	2.2	95%
SparseDiff	1.6 $\pm$ 0.9	5.0 $\pm$ 0.1	4.5 $\pm$ 0.9	1.7 $\pm$ 0.5	75% $\pm$ 10	0.3 $\pm$ 0.0	3.2 $\pm$ 0.3	0.1 $\pm$ 0.1	1.2 $\pm$ 0.4	85% $\pm$ 9

computed with  $\text{MMD}(\text{train}, \text{test})^2$ , are used as the reference and represented by a light gray line. Detailed results with higher precision are available in Appendix C.3 for facilitating comparison.

**Results** The results of large and synthetic graph generation are depicted in Tables 1 and 2. While dense models like DiGress (Vignac et al., 2023a) perform excellently on SBM and planar graphs, those models struggle with larger datasets such as Ego and Protein due to quadratic space complexity. Dense graph diffusion models are limited to very small batch sizes (e.g., 2 on a 32GB GPU), resulting in slow training and poor convergence. In contrast, SparseDiff supports much larger batch sizes during training, thanks to the controllable sparsity parameter  $\lambda$ . Consequently, its performance matches previous dense and sparse models on mid-sized datasets like SBM and Planar and remains highly competitive with scalable models across various metrics on larger datasets such as Ego and Protein. Besides, we observe that our method consistently achieves the best results on the aggregated average ratio metrics, thereby validating its globally superior performance.

## 4.2 MOLECULE GENERATION

Given that our method behaves like dense models in the limit case where  $\lambda = 1$ , it is expected to align with their performance on small graph datasets. We evaluate our approach using the QM9 and Moses molecular datasets, anticipating its performance comparable to that of dense models. The QM9 dataset (Wu et al., 2018) features molecules with up to 9 heavy atoms, while the Moses benchmark (Polykovskiy et al., 2020), derived from ZINC Clean Leads, includes drug-sized molecules with extensive assessment tools. In QM9, we add formal charges as discrete node features during diffusion, similar to Vignac et al. (2023b), and apply the same to DiGress for consistency. We assess molecular performance by the proportion of connected graphs, validity of the largest connected component verified by RDKit, and uniqueness of over 10,000 molecules. Additionally, we use the Frechet ChemNet Distance (FCD) (Preuer et al., 2018) to measure molecular similarity, excluding 0.96% of invalid molecules for FCD analysis.

Table 3 demonstrates that SparseDiff consistently outperforms other scalable methods on the FCD metric, highlighting its effectiveness for small, structured graphs even without significant sparsity advantages. Additionally, SparseDiff achieves results comparable to the state-of-the-art dense

Table 3: Molecule generation on QM9 with implicit hydrogens. Validity, uniqueness, and connectivity metrics are reported as percentages.

Dense Models				—	Sparse Models				
Model	Valid $\uparrow$	Unique $\uparrow$	Conn. $\uparrow$	FCD $\downarrow$	Model	Valid $\uparrow$	Unique $\uparrow$	Conn. $\uparrow$	FCD $\downarrow$
SPECTRE	87.3	35.7	-	-	GraphARM	90.3	-	-	1.22
GraphNVP	83.1	99.2	-	-	EDGE	99.1	<b>100</b>	-	0.46
GDSS	95.7	98.5	-	2.9	HGGT	99.2	95.7	-	0.40
DiGress	<b>99.3<math>\pm</math>0.0</b>	<b>95.9<math>\pm</math>0.2</b>	<b>99.4<math>\pm</math>0.2</b>	<b>0.15<math>\pm</math>0.01</b>	SparseDiff	<b>99.2<math>\pm</math>0.1</b>	<b>96.4<math>\pm</math>0.1</b>	<b>99.8<math>\pm</math>0.1</b>	<b>0.12<math>\pm</math>0.00</b>

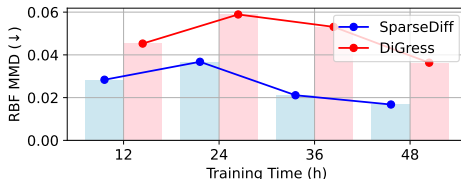
model, DiGress, across other metrics. Additional results for QM9 with explicit hydrogens and the Moses dataset (Tables 9 and 10 in Appendices D.2 and D.3) confirm that SparseDiff matches or exceeds the performance of the state-of-the-art model across various molecular datasets. We further validate the robust performance of SparseDiff under different sparsity parameters  $\lambda$  to confirm its stability (Tables 12 in Appendix D.5).

### 4.3 EFFICIENCY ANALYSIS

Table 4: Convergence comparison of graph diffusion models after 24 hours of training.

Model	Deg. $\downarrow$	Clust. $\downarrow$	Orbit $\downarrow$	Ratio $\downarrow$	RBF $\downarrow$
EDP-GNN	22	36	9.9	59	-
DiGress	4.0	4.9	<b>3.4</b>	11	5.6
EDGE	46	18	4.5	87	3.6
GraphLE	58	23	4.2	110	-
SparseDiff	<b>2.3</b>	<b>4.7</b>	3.6	<b>7.8</b>	<b>3.5</b>

Figure 5: Convergence comparison between DiGress and SparseDiff.



**Training efficiency** We compare SparseDiff’s performance on the Ego dataset against other diffusion models, including dense models like EDP-GNN and DiGress, and sparse models such as EDGE and GraphLE. Table 4 shows that after 24 hours of training on a V100-32G machine, SparseDiff outperforms all metrics except for a minor increase in Orbit MMD compared to DiGress. The comparison of graph diffusion models’ sampling speeds is further presented in Table 11 in Appendix D.4. Figure 5 shows that SparseDiff has a significantly faster convergence speed compared to DiGress, achieving satisfactory results within two days. Notably, a SparseDiff model trained for 12 hours demonstrates an RBF MMD comparable to a DiGress model trained for 48 hours.

**Inference efficiency** We test the Ego and Planar datasets with different numbers of inference steps (1000, 500, and 200) after training with  $T = 1,000$  steps. The results, presented in Table 5, surprisingly demonstrate that even with a 5-fold increase in generation speed (down to 200 steps), our model keeps to be performing, and consistently outperforms most other dense and scalable models.

Table 5: Inference acceleration results.

Dataset	Steps	Deg. $\downarrow$	Clust. $\downarrow$	Orbit $\downarrow$	Ratio $\downarrow$	RBF $\downarrow$
Ego	1000	3.6	3.1	1.5	8.2	2.0
	500	2.3	2.9	2.0	6.2	2.1
	200	3.7	3.1	1.6	8.4	2.3
Dataset	Steps	Deg.	Clust.	Orbit	Ratio	V.U.N
Planar	1000	0.3	3.2	0.1	1.2	85%
	500	0.3	3.4	0.2	1.5	80%
	200	0.5	3.7	0.4	2.6	69%

## 5 CONCLUSION

In this work, we introduce SparseDiff, a scalable discrete denoising diffusion model for graph generation. SparseDiff allows precise control over computational resources by predicting only a subset of edges at once. Experimental results demonstrate its superior and robust performance across graphs of all sizes, extending its applicability to tasks such as generating large molecules and community graphs. While SparseDiff meets most requirements of most scenarios, its scalability and ability to generate graphs with out-of-distribution node counts could be enhanced by incorporating a structured hierarchical approach. This enhancement promises to broaden its applicability in more complex graph generation tasks.

## REFERENCES

- Uri Alon and Eran Yahav. On the bottleneck of graph neural networks and its practical implications. *arXiv preprint arXiv:2006.05205*, 2020. 6
- Jacob Austin, Daniel Johnson, Jonathan Ho, Daniel Tarlow, and Rianne van den Berg. Structured denoising diffusion models in discrete state-spaces. In *Advances in Neural Information Processing Systems*, volume 34, 2021. 2, 4, 7
- Minkyung Baek, Frank DiMaio, Ivan Anishchenko, Justas Dauparas, Sergey Ovchinnikov, Gyu Rie Lee, Jue Wang, Qian Cong, Lisa N Kinch, R Dustin Schaeffer, et al. Accurate prediction of protein structures and interactions using a three-track neural network. *Science*, 373(6557):871–876, 2021. 2
- Albert-László Barabási. Network science. *Philosophical Transactions of the Royal Society A: Mathematical, Physical and Engineering Sciences*, 371(1987), 2013. 1
- Andreas Bergmeister, Karolis Martinkus, Nathanaël Perraudin, and Roger Wattenhofer. Efficient and scalable graph generation through iterative local expansion. *arXiv preprint arXiv:2312.11529*, 2023. 1, 2, 8
- Armand Boschin. *Machine learning techniques for automatic knowledge graph completion*. PhD thesis, Institut polytechnique de Paris, 2023. 5
- Benjamin Paul Chamberlain, Sergey Shirobokov, Emanuele Rossi, Fabrizio Frasca, Thomas Markovich, Nils Hammerla, Michael M Bronstein, and Max Hansmire. Graph neural networks for link prediction with subgraph sketching. *arXiv preprint arXiv:2209.15486*, 2022. 5
- Xiaohui Chen, Jiaying He, Xu Han, and Li-Ping Liu. Efficient and degree-guided graph generation via discrete diffusion modeling. *arXiv preprint arXiv:2305.04111*, 2023. 1, 2, 3, 8
- Zhengdao Chen, Lei Chen, Soledad Villar, and Joan Bruna. Can graph neural networks count substructures? In *Advances in neural information processing systems*, volume 33, 2020. 16
- Gabriele Corso, Luca Cavalleri, Dominique Beaini, Pietro Liò, and Petar Veličković. Principal neighbourhood aggregation for graph nets. *Advances in Neural Information Processing Systems*, 2020. 6, 15
- Hanjun Dai, Azade Nazi, Yujia Li, Bo Dai, and Dale Schuurmans. Scalable deep generative modeling for sparse graphs. In *International Conference on Machine Learning*. PMLR, 2020. 1, 8
- Nicola De Cao and Thomas Kipf. Molgan: An implicit generative model for small molecular graphs. In *ICML Workshop on Theoretical Foundations and Applications of Deep Generative Models*, 2018. 1
- Agnés Desolneux, Lionel Moisan, and Jean-Michel Morel. Estimating the binomial tail. *From Gestalt Theory to Image Analysis: A Probabilistic Approach*, pp. 47–63, 2008. 4, 15
- Prafulla Dhariwal and Alexander Nichol. Diffusion models beat gans on image synthesis. In *Advances in Neural Information Processing Systems*, 2021. 2
- Francesco Di Giovanni, Lorenzo Giusti, Federico Barbero, Giulia Luise, Pietro Lio, and Michael M. Bronstein. On over-squashing in message passing neural networks: The impact of width, depth, and topology. In *Proceedings of the 40th International Conference on Machine Learning*, 2023. 6
- Paul Erdős, Alfréd Rényi, et al. On the evolution of random graphs. *Publ. math. inst. hung. acad. sci.*, 1960. 1
- Matthias Fey and Jan Eric Lenssen. Fast graph representation learning with pytorch geometric. *arXiv preprint arXiv:1903.02428*, 2019. 3, 5

- Justin Gilmer, Samuel S Schoenholz, Patrick F Riley, Oriol Vinyals, and George E Dahl. Neural message passing for quantum chemistry. In *International conference on machine learning*. PMLR, 2017. 5
- Kilian Konstantin Haefeli, Karolis Martinkus, Nathanaël Perraudin, and Roger Wattenhofer. Diffusion models for graphs benefit from discrete state spaces. *arXiv preprint arXiv:2210.01549*, 2022. 2
- Jonathan Ho, Ajay Jain, and Pieter Abbeel. Denoising diffusion probabilistic models. In *Advances in Neural Information Processing Systems*. Curran Associates, Inc., 2020. 2
- Jonathan Ho, William Chan, Chitwan Saharia, Jay Whang, Ruiqi Gao, Alexey Gritsenko, Diederik P Kingma, Ben Poole, Mohammad Norouzi, David J Fleet, et al. Imagen video: High definition video generation with diffusion models. *arXiv preprint arXiv:2210.02303*, 2022. 2
- John Ingraham, Max Baranov, Zak Costello, Vincent Frappier, Ahmed Ismail, Shan Tie, Wujie Wang, Vincent Xue, Fritz Obermeyer, Andrew Beam, et al. Illuminating protein space with a programmable generative model. *bioRxiv*, 2022. 2
- Yunhui Jang, Dongwoo Kim, and Sungsoo Ahn. Hierarchical graph generation with k2-trees. *arXiv preprint arXiv:2305.19125*, 2023. 1, 2, 8
- Wengong Jin, Regina Barzilay, and Tommi Jaakkola. Junction tree variational autoencoder for molecular graph generation. In *International conference on machine learning*. PMLR, 2018. 2
- Wengong Jin, Regina Barzilay, and Tommi Jaakkola. Hierarchical generation of molecular graphs using structural motifs. In *International Conference on Machine Learning*. PMLR, 2020. 2
- Jaehyeong Jo, Seul Lee, and Sung Ju Hwang. Score-based generative modeling of graphs via the system of stochastic differential equations. *arXiv preprint arXiv:2202.02514*, 2022. 1, 2, 4, 8
- Jaehyeong Jo, Dongki Kim, and Sung Ju Hwang. Graph generation with destination-predicting diffusion mixture. *arXiv preprint arXiv:2302.03596*, 2023. 8
- Mahdi Karami. Higen: Hierarchical graph generative networks. *arXiv preprint arXiv:2305.19337*, 2023. 1, 2, 8
- Lingkai Kong, Jiaming Cui, Haotian Sun, Yuchen Zhuang, B. Aditya Prakash, and Chao Zhang. Autoregressive diffusion model for graph generation, 2023. URL <https://openreview.net/forum?id=98J48HZXxd5>. 1, 3, 8
- Zhifeng Kong, Wei Ping, Jiaji Huang, Kexin Zhao, and Bryan Catanzaro. Diffwave: A versatile diffusion model for audio synthesis. *arXiv preprint arXiv:2009.09761*, 2020. 2
- Xujia Li, Yuan Li, Xueying Mo, Hebing Xiao, Yanyan Shen, and Lei Chen. Diga: Guided diffusion model for graph recovery in anti-money laundering. In *Proceedings of the 29th ACM SIGKDD Conference on Knowledge Discovery and Data Mining*, 2023. 1
- Renjie Liao, Yujia Li, Yang Song, Shenlong Wang, Charlie Nash, William L. Hamilton, David Duvenaud, Raquel Urtasun, and Richard Zemel. Efficient graph generation with graph recurrent attention networks. In *NeurIPS*, 2019. 3, 8
- Stratis Limnios, Praveen Selvaraj, Mihai Cucuringu, Carsten Maple, Gesine Reinert, and Andrew Elliott. Sages: Sampling graph denoising diffusion model for scalable graph generation. *arXiv preprint arXiv:2306.16827*, 2023. 1, 3, 18
- Qi Liu, Miltiadis Allamanis, Marc Brockschmidt, and Alexander Gaunt. Constrained graph variational autoencoders for molecule design. *Advances in neural information processing systems*, 31, 2018. 3
- Kaushalya Madhawa, Katushiko Ishiguro, Kosuke Nakago, and Motoki Abe. Graphnvp: An invertible flow model for generating molecular graphs. *arXiv preprint arXiv:1905.11600*, 2019. 8

- Karolis Martinkus, Andreas Loukas, Nathanaël Perraudin, and Roger Wattenhofer. Spectre: Spectral conditioning helps to overcome the expressivity limits of one-shot graph generators. *arXiv preprint arXiv:2204.01613*, 2022. [2](#), [8](#), [16](#), [17](#)
- Krzysztof Maziarz, Henry Richard Jackson-Flux, Pashmina Cameron, Finton Sirockin, Nadine Schneider, Nikolaus Stiefl, Marwin Segler, and Marc Brockschmidt. Learning to extend molecular scaffolds with structural motifs. In *International Conference on Learning Representations (ICLR)*, 2022. [2](#)
- Rocío Mercado, Tobias Rastemo, Edvard Lindelöf, Günter Klambauer, Ola Engkvist, Hongming Chen, and Esben Jannik Bjerrum. Graph networks for molecular design. *Machine Learning: Science and Technology*, 2021. [3](#)
- Chenhao Niu, Yang Song, Jiaming Song, Shengjia Zhao, Aditya Grover, and Stefano Ermon. Permutation invariant graph generation via score-based generative modeling. In *International Conference on Artificial Intelligence and Statistics*. PMLR, 2020. [1](#), [2](#), [4](#)
- Ethan Perez, Florian Strub, Harm De Vries, Vincent Dumoulin, and Aaron Courville. Film: Visual reasoning with a general conditioning layer. In *Proceedings of the AAAI Conference on Artificial Intelligence*, volume 32, 2018. [6](#), [15](#)
- Daniil Polykovskiy, Alexander Zhebrak, Benjamin Sanchez-Lengeling, Sergey Golovanov, Oktai Tatanov, Stanislav Belyaev, Rauf Kurbanov, Aleksey Artamonov, Vladimir Aladinskiy, Mark Veselov, et al. Molecular sets (moses): a benchmarking platform for molecular generation models. In *Frontiers in pharmacology*. Frontiers Media SA, 2020. [9](#)
- Kristina Preuer, Philipp Renz, Thomas Unterthiner, Sepp Hochreiter, and Gunter Klambauer. Fréchet chemnet distance: a metric for generative models for molecules in drug discovery. *Journal of chemical information and modeling*, 58(9):1736–1741, 2018. [9](#)
- Can Rong, Jingtao Ding, Zhicheng Liu, and Yong Li. City-wide origin-destination matrix generation via graph denoising diffusion. *arXiv preprint arXiv:2306.04873*, 2023. [1](#)
- Franco Scarselli, Marco Gori, Ah Chung Tsoi, Markus Hagenbuchner, and Gabriele Monfardini. The graph neural network model. In *IEEE transactions on neural networks*. IEEE, 2008. [5](#)
- Yunsheng Shi, Zhengjie Huang, Shikun Feng, Hui Zhong, Wenjin Wang, and Yu Sun. Masked label prediction: Unified message passing model for semi-supervised classification. *arXiv preprint arXiv:2009.03509*, 2020. [6](#), [15](#)
- Martin Simonovsky and Nikos Komodakis. Graphvae: Towards generation of small graphs using variational autoencoders. In *International conference on artificial neural networks*. Springer, 2018. [1](#)
- Jiaming Song, Chenlin Meng, and Stefano Ermon. Denoising diffusion implicit models. *arXiv preprint arXiv:2010.02502*, 2020. [7](#)
- Rylee Thompson, Boris Knyazev, Elahe Ghalebi, Jungtaek Kim, and Graham W Taylor. On evaluation metrics for graph generative models. *arXiv preprint arXiv:2201.09871*, 2022. [8](#), [17](#)
- Jake Topping, Francesco Di Giovanni, Benjamin Paul Chamberlain, Xiaowen Dong, and Michael M Bronstein. Understanding over-squashing and bottlenecks on graphs via curvature. *arXiv preprint arXiv:2111.14522*, 2021. [6](#)
- Petar Veličković, Guillem Cucurull, Arantxa Casanova, Adriana Romero, Pietro Lio, and Yoshua Bengio. Graph attention networks. *arXiv preprint arXiv:1710.10903*, 2017. [6](#), [15](#)
- Clement Vignac, Igor Krawczuk, Antoine Siraudin, Bohan Wang, Volkan Cevher, and Pascal Frossard. Digress: Discrete denoising diffusion for graph generation. In *The Eleventh International Conference on Learning Representations*, 2023a. [1](#), [2](#), [4](#), [5](#), [8](#), [9](#), [15](#)
- Clément Vignac, Nagham Osman, Laura Toni, and Pascal Frossard. Midi: Mixed graph and 3d denoising diffusion for molecule generation. In *ECML/PKDD*, 2023b. [3](#), [9](#), [16](#)

- Minjie Yu Wang. Deep graph library: Towards efficient and scalable deep learning on graphs. In *ICLR workshop on representation learning on graphs and manifolds*, 2019. [5](#)
- Zhenqin Wu, Bharath Ramsundar, Evan N. Feinberg, Joseph Gomes, Caleb Geniesse, Aneesh S. Pappu, Karl Leswing, and Vijay Pande. Moleculenet: a benchmark for molecular machine learning. In *Chem. Sci.* The Royal Society of Chemistry, 2018. [9](#)
- Shuai Yang, Xipeng Shen, and Seung-Hwan Lim. Revisit the scalability of deep auto-regressive models for graph generation. In *2021 International Joint Conference on Neural Networks (IJCNN)*, 2021. [2](#)
- Jiaxuan You, Rex Ying, Xiang Ren, William Hamilton, and Jure Leskovec. Graphrnn: Generating realistic graphs with deep auto-regressive models. In *International conference on machine learning*. PMLR, 2018. [8](#)
- Muhan Zhang and Yixin Chen. Link prediction based on graph neural networks. In *Advances in neural information processing systems*, volume 31, 2018. [5](#)

## A PROOF OF LEMMA 3.1

The lemma for a noisy graph with guaranteed sparsity comes directly from the proposition regarding the tail behavior of a binomial distribution (Desolneux et al., 2008) as follows:

**Proposition A.1.** (Tail behavior of a binomial distribution)

Let  $X_i, i = 1, \dots, l$  be independent Bernoulli random variables with parameter  $0 < p < \frac{1}{4}$  and let  $S_l = \sum_{i=1}^l X_i$ . Consider a constant  $p < r < 1$  or a real function  $p < r(l) < 1$ . Then according to the Hoeffding inequality,  $\mathcal{B}(l, k, p) = \mathbb{P}[S_l \geq k]$  satisfies:

$$-\frac{1}{l} \log \mathcal{P}[S_l \geq rl] \geq r \log \frac{r}{p} + (1-p) \log \frac{1-r}{1-p} \quad (3)$$

For sparse graphs, the edge ratio  $r$  is clearly smaller than  $\frac{1}{4}$ . Consider then Bernoulli random variables with the parameter  $r$  and a noised edge ratio  $r < k < 1$  with  $l = n(n-1)/2$  (i.e. number of all node pairs in an undirected graph without self-loops) draws, and note the sampled ‘existing’ edge number  $S_{n(n-1)/2}$  as  $m_t$ , we have:

$$\log(\mathbb{P}[r_t = \frac{m_t}{n(n-1)/2} \geq k]) \leq -\frac{n(n-1)}{2} [k \log \frac{k}{r} + (1-r) \log \frac{1-k}{1-r}] \quad (4)$$

## B MODEL ARCHITECTURE

Our sparse denoising network adopts the graph transformer architecture Veličković et al. (2017), featuring normalization, feed-forward, and attention layers. To handle sparse data, it incorporates the sparse attention mechanism (Shi et al., 2020) based on weighted message-passing layers and integrates enhancements from Vignac et al. (2023a), such as PNA pooling layers (Corso et al., 2020) and FiLM layers (Perez et al., 2018).

Precisely, we introduce the FiLM layer and the PNA layer inside the model architecture to enhance its performance. Precisely, the FiLM layer is used to combine features at different scales, such as node and edge features. Specifically, given two features  $M_1$  and  $M_2$ , and trainable parameters  $W_1$  and  $W_2$ , the FiLM layer output is calculated as  $\text{FiLM}(M_1, M_2) = M_1 W_1 + (M_1 W_2) \odot M_2 + M_2$ . As an illustration, within the convolutional layer, the graph feature  $M_2$  is integrated with edge features  $M_1$  to enhance predictions. While PNA layer is used as a specialized pooling layer to obtain information from different dimensions of a specific feature. Given the feature  $X$  and trainable parameter  $W$ ,  $\text{PNA}(X) = \text{cat}(\max(X), \min(X), \text{mean}(X), \text{std}(X)) W$ . For example, node features  $X$  are forwarded to a PNA layer for extracting global information across different scales, which is subsequently added to the graph feature to enhance its representation.

Finally, we enrich the message-passing graph with additional encodings, such as the graph Laplacian and cycle counts, to enhance structural and positional information (detailed in Appendix B.1). These encodings can only be computed effectively when the noisy graphs are sparse, which is another significant advantage of discrete diffusion models using marginal transitions. It is worth noting that not all these encodings can be computed in sub-quadratic time. However, in practice, this does not pose an issue as they are not used for back-propagation, which arises as the primary complexity bottleneck during training. For instance, for the large Protein dataset, computing these encodings is five times faster than the forward pass itself. Nevertheless, on very larger graphs, expensive ones should not be computed.

### B.1 ADDITIONAL ENCODINGS

During training, we augment model expressiveness with additional encodings. To make things clear, we divide them into encodings for edges, nodes, and for graphs.

**Encoding for graphs** We first incorporate graph eigenvalues, known for their critical structural insights, and cycle counts, addressing message-passing neural networks’ inability to detect cycles

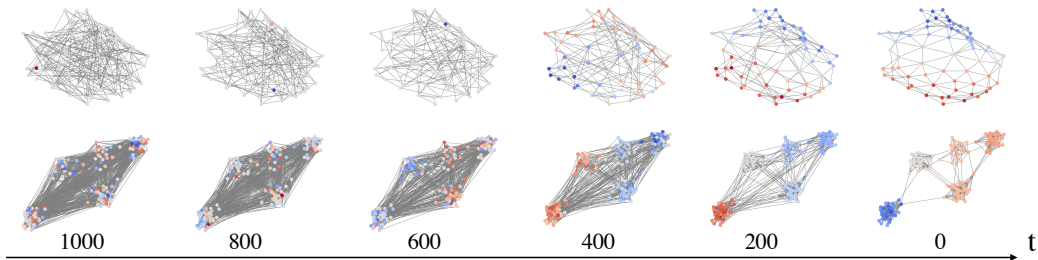


Figure 6: Visualization of iterative generation for Planar and SBM graphs.

(Chen et al., 2020). The first requires  $n^3$  operations for matrix decomposition, the second requires  $n^2$  for matrix multiplication, but both are optional in our model and do not significantly limit scalability even with graphs up to size 500. In addition to the previously mentioned structural encodings, we integrate the degree distribution to enhance the positional information within the graph input, which is particularly advantageous for graphs with central nodes or multiple communities. Furthermore, for graphs featuring attributed nodes and edges, the inclusion of node type and edge type distributions also provides valuable benefits.

**Encoding for nodes** At the node level, we use graph eigenvectors, which are fundamental in graph theory, offering valuable insights into centrality, connectivity, and diverse graph properties.

**Encoding for edges** To aid in edge label prediction, we introduce auxiliary structural encodings related to edges. These include the shortest distance between nodes and the Adamic-Adar index. The former enhances node interactions, while the latter focuses on local neighborhood information. Due to computational constraints, we consider information within a 10-hop radius, categorizing it as local positional information.

**Molecular information** In molecular datasets, we augment node features by incorporating edge valency and atom weights. Additionally, formal charge information is included as an additional node label for diffusion and denoising during training, as formal charges have been experimentally validated as valuable information (Vignac et al., 2023b).

## C EXPERIMENTAL SETUP

In our experimental setup, we utilize a single V100-32G GPU machine, which is particularly prone to scalability issues, to demonstrate that our method allows users with limited GPU resources to effectively train on larger graphs. Detailed specifications regarding workers, memory allocation, execution time, and optimizers are meticulously indicated in the configuration details provided in our code.

As for dataset splits, we adhere to the framework established by DiGress. Specifically, for the QM9 dataset, we implement a split comprising 100k molecules for training, 20k for validation, and 13k for evaluating likelihood on the test set. For the Planar, SBM, and Protein datasets, employing a seed of 1234, we randomly assign 20% of the graphs to testing, while 80% of the remaining graphs are utilized for training, and 20% for validation. For the Ego dataset, to ensure consistency with previous methods and a fair comparison, we maintain a split of 80% for training and 20% for testing, with 20% of the training set additionally used for validation purposes. All configuration details are comprehensively documented in the code provided.

### C.1 MMD METRICS

In our research, we carefully select specific metrics tailored to each dataset, with a primary focus on four widely recognized Maximum Mean Discrepancy (MMD) metrics. These metrics use the total variation (TV) distance, as detailed in Martinkus et al. (2022). They encompass node degree (Deg), clustering coefficient (Clus), orbit count (Orb), and graph spectra (Spec). The first three local metrics compare the degree distributions, clustering coefficient distributions, and the occurrence of all

4-node orbits within graphs between the generated and training samples. Additionally, the comparison of graph spectra is realized by computing the eigenvalues of the normalized graph Laplacian, providing complementary insights into the global properties of the graphs.

### C.2 STATISTICS OF THE DATASETS

Table 6: Statistics for the datasets employed in our experiments.

Name	Graph number	Node range	Edge range	Edge Ratio (%)	$\lambda$ (%)
QM9	133,885	[2,9]	[2, 28]	[20, 56]	100
QM9(H)	133,885	[3, 29]	[4, 56]	[7.7, 44]	50
Moses	1,936,962	[8, 27]	[14, 62]	[8.0, 22]	50
Planar	200	[64, 64]	[346, 362]	[8.4, 8.8]	50
SBM	200	[44, 187]	[258, 2258]	[6.0, 17]	25
Ego	757	[50, 399]	[112, 2124]	[1.2, 11]	10
Protein	918	[100, 500]	[372, 3150]	[8.9, 6.7]	10

To provide a more comprehensive overview of the various scales found in ‘existing’ graph datasets, we present here key statistics for them. These statistics encompass the number of graphs, the range of node numbers, the range of edge numbers, the edge ratio for ‘existing’ edges, and the sparsity parameter  $\lambda$  used for training, i.e. the proportion of ‘existing’ edges among all node pairs. In our consideration, we focus on undirected graphs. Therefore, when counting edges between nodes  $i$  and  $j$ , we include the edge in both directions.

### C.3 RAW RESULTS

Table 7: Raw results on the SBM, Planar, Protein, and Ego datasets.

Model	Deg. (e-3)↓	Clust. (e-2)↓	Orbit (e-2)↓	Spec. (e-3)↓	FID↓	RBF MMD (e-2)↓
<i>SBM</i>						
Training set	0.85	3.32	2.55	2.74	1.37	3.23
SparseDiff	1.57±0.91	5.04±0.06	4.51±0.90	6.68±2.04	4.55±2.01	4.98±0.06
<i>Planar</i>						
Training set	0.19	3.10	0.05	3.82	1.57	8.89
SparseDiff	0.32±0.01	3.25±0.35	0.09±0.08	6.99±0.92	2.94±3.15	9.84±0.91
<i>Protein</i>						
Training set	0.32	0.68	0.32	0.49	1.36	1.37
SparseDiff	1.45±0.30	3.35±0.33	0.53±0.78	1.35±0.16	5.97±1.07	3.77±0.65
<i>Ego</i>						
Training set	0.16	0.71	0.69	0.98	0.07	0.86
SparseDiff	3.70±0.44	3.18±0.10	1.98±0.42	5.63±0.80	4.84±1.56	2.60±0.31

To ease comparison with other methods, Table 7 provides the raw numbers (not presented as ratios) for the SBM, Planar, Ego, and Protein datasets. Note that this table contains the FID metrics from Thompson et al. (2022), which we did not include in the main text. The reason is that we found this metric to be very brittle, with some evaluations giving a very large value that would dominate the mean results. Besides, we have identified a discrepancy in the Spectre metrics reported in the study by Martinkus et al. (2022) when computed under non-parallel computation. We thus provide the updated values for reference and use the updated value for ratio calculation in Table 2 and in Table 1. The checkpoints needed to reproduce the results mentioned can be accessed via the provided URL. The code is available at <https://github.com/qym7/SparseDiff>. The checkpoints for reproducing the results above can be found at <https://drive.switch.ch/index.php/s/1hHNVCb0ylbYPoQ>.

## D ADDITIONAL EXPERIMENTS

### D.1 TRAINING WITH GRAPH OF OVER 1000 NODES

Table 8: Large graph generation on the Facebook dataset. Triangles and squares are abbreviated as ‘tri’ and ‘squ’ in the table, while PLE represents power law exp.

Model	num nodes	num edges	num tri	num squ	max deg	clust	assort	PLE	CPL
Real	1045	27,755	446,846	34,098,662	1044	0.57579	-0.02543	1.28698	1.94911
SaGess	1043	<b>27,758</b>	429,428	35,261,545	999	<b>0.52098</b>	-0.01607	1.29003	2.00800
SparseDiff	<b>1045</b>	27,763	<b>446,819</b>	<b>34,095,513</b>	<b>1044</b>	0.43310	<b>-0.02536</b>	<b>1.28687</b>	<b>1.94921</b>

We trained on the largest graph with 1045 nodes from the Facebook dataset, following the SaGess (Limnios et al., 2023) setting. SparseDiff was evaluated using SaGess metrics as a reference. However, employing the same graph for both training and evaluating test metrics entails potential risks, as perfect metrics may result from overfitting to the training graph. In the provided table, we present SaGess-RW, demonstrating the best results among the three proposed SaGess models. Notably, SaGess generates small graphs and concatenates them to meet the required number of edges, while SparseDiff generates a single large graph based on the specified node count. This explains SparseDiff’s advantage in the ‘num nodes’ metric and SaGess’s advantage in the ‘num edges’ metric. Furthermore, SparseDiff closely aligns with real data statistics, except for the clustering coefficient, showcasing not only its scalability up to 1000 nodes but also its strong performance on such single-graph datasets.

### D.2 QM9 WITH EXPLICIT HYDROGENS

Table 9: Unconditional generation on QM9 with explicit hydrogens. On small graphs such as QM9, sparse models are not beneficial, but SparseDiff still achieves very good performance.

Model	Connected	Valid $\uparrow$	Unique $\uparrow$	Atom stable $\uparrow$	Mol stable $\uparrow$
DiGress	-	95.4	<b>97.6</b>	98.1	79.8
DiGress + charges	<b>98.6</b>	97.7	96.9	99.8	97.0
SparseDiff(ours)	98.3 $\pm$ .08	<b>97.9<math>\pm</math>.13</b>	97.4 $\pm$ .10	-	-

We additionally report the results for QM9 with explicit hydrogens in Table 9. Having explicit hydrogens makes the problem more complex because the resulting graphs are larger. We observe that SparseDiff achieves better validity than DiGress and has comparable results on other metrics when both are utilizing charges.

## D.3 MOSES BENCHMARK EVALUATION

Table 10: Mean and standard deviation across 5 samplings on the Moses benchmark. SparseDiff has a similar performance to DiGress, despite a shorter training time.

Model	Connected $\uparrow$	Valid (%) $\uparrow$	Unique (%) $\uparrow$	Novel (%) $\uparrow$	Filters (%) $\uparrow$
GraphINVENT	–	<b>96.4</b>	99.8	–	95.0
DiGress	–	85.7	<b>100.0</b>	95.0	<b>97.1</b>
SparseDiff	94.8 $\pm$ 1	84.7 $\pm$ 2	<b>100.0<math>\pm</math>0</b>	<b>95.1<math>\pm</math>1</b>	<b>97.0<math>\pm</math>2</b>
Model	FCD $\downarrow$	SNN (%) $\uparrow$	Scaf (%) $\uparrow$	Frag (%) $\uparrow$	IntDiv (%) $\uparrow$
GraphINVENT	1.22	<b>53.9</b>	12.7	98.6	<b>85.7</b>
DiGress	<b>1.19</b>	52.2	<b>14.8</b>	99.6	85.3
SparseDiff	1.28 $\pm$ 0.1	52.2 $\pm$ 0	<b>15.5<math>\pm</math>1.3</b>	<b>99.8<math>\pm</math>0</b>	85.4 $\pm$ 0
Model	IntDiv2 (%) $\uparrow$	logP ( $e^{-2}$ ) $\downarrow$	SA( $e^{-2}$ ) $\downarrow$	QED ( $e^{-3}$ ) $\downarrow$	Weight (%) $\downarrow$
GraphINVENT	<b>85.1</b>	<b>0.67</b>	4.5	<b>0.25</b>	16.1
DiGress	–	3.4	<b>3.6</b>	2.91	<b>1.42</b>
SparseDiff	84.8 $\pm$ 0	3.0 $\pm$ 3	5.4 $\pm$ 2	1.21 $\pm$ 21	5.58 $\pm$ 15

Moses is an extensive molecular dataset with larger molecular graphs than QM9, offering a much more comprehensive set of metrics. While autoregressive models such as GraphINVENT are recognized for achieving higher validity on this dataset, both SparseDiff and DiGress exhibit advantages across most other metrics. Notably, SparseDiff closely aligns with the results achieved by DiGress, affirming the robustness of our method on complex datasets.

## D.4 SAMPLING SPEED COMPARISON

Table 11: Sampling speed for generating 8 Ego graphs.

Model	EDP-GNN	DiGress	EDGE	GraphLE	SparseDiff	SparseDiff (200 steps)
Time (min)	5	32	2	20	28	5

The speed of generating 8 Ego graphs is demonstrated in Table 11. Notably, for GraphLE, the batch size is constrained to 2 due to its substantial memory requirements. An additional column labeled ‘‘SparseDiff (200 steps)’’ represents the sampling time after reducing the inference steps from 1,000 to 200 through acceleration strategies. The table illustrates that SparseDiff maintains comparable speed to dense models without significant compromise on space efficiency and can be significantly accelerated during sampling.

## D.5 INFLUENCE OF THE SPARSITY PARAMETER

Table 12: Unconditional generation on QM9 under different sparsity parameters  $\lambda$ .

$\lambda$	Valid $\uparrow$	Unique $\uparrow$	Connected $\uparrow$	FCD $\downarrow$
100%	99.23 $\pm$ 0.06	96.37 $\pm$ 0.13	99.76 $\pm$ 0.06	0.117 $\pm$ 0.004
50%	99.12 $\pm$ 0.05	96.80 $\pm$ 0.18	99.61 $\pm$ 0.05	0.107 $\pm$ 0.007
25%	99.16 $\pm$ 0.06	96.54 $\pm$ 0.19	99.59 $\pm$ 0.06	0.119 $\pm$ 0.006
10%	99.11 $\pm$ 0.09	96.89 $\pm$ 0.15	99.61 $\pm$ 0.01	0.105 $\pm$ 0.004

Table 12 above shows the results of unconditional generation on the QM9 dataset under different sparsity parameters ( $\lambda$ ). The performance of SparseDiff remains consistent across various  $\lambda$  values, with metrics for connectivity, validity, uniqueness, and Frechet ChemNet Distance (FCD) showing minimal changes from 100% to 10%  $\lambda$ . For example, the validity metric stays between 99.12% and 99.23%, and uniqueness ranges from 96.37% to 96.89%. We remark that, for  $\lambda$  values of 10%

and 25%, the model was trained for twice as many epochs since the cross-entropy loss considers fewer edges per epoch, necessitating more epochs for convergence. Despite this, all models exhibit consistent performance across different  $\lambda$  values after convergence, which highlights the robustness and stability of SparseDiff in generating high-quality molecular graphs.

## D.6 ABLATIONS

This part presents 2 ablation experiments that motivate our approach. SparseDiff builds upon an experimental observation and a hypothesis. Firstly, our experiments demonstrate that relying solely on node features for link prediction yields unsatisfactory results. This observation encouraged us to design the message-passing graph that contains all edges to be predicted (i.e. query edges) as the message-passing graph to directly obtain their edge features. Secondly, we hypothesized that preserving the same distribution of edge types as observed in dense graphs for loss calculation is advantageous for training. This hypothesis necessitates the sampling of query edges within each graph in a batch of graphs with varying sizes, thereby introducing increased complexity to the algorithm design process.

### D.6.1 LINK PREDICTION

Table 13: Influence of including edges features for edge prediction.

Model	Deg ↓	Clus ↓	Orb ↓	Spec ↓	FID ↓	RBF MMD ↓
Link Pred	0.0043	0.0721	<b>0.0275</b>	0.0344	1.51e6	<b>0.0315</b>
SparseDiff	<b>0.0019±.00</b>	<b>0.0537±.00</b>	0.0299±.00	<b>0.0050±.00</b>	<b>16.1±12.9</b>	0.0483±.01

In this experiment, we intentionally avoided using easily learnable molecular datasets that come with rich supplementary encodings. Instead, we chose to conduct the experiments on a large dataset, namely Ego, to assess their performance. In Table 13, a model that does not specifically include edge features for edge prediction performs much worse on all metrics except on RBF MMD and orbit. This observation shows that, despite that a model can also leverage the information of ‘existing’ edges into node features, the lack of edge features during training deteriorates significantly models’ performance.

### D.6.2 QUERY EDGES WITH PROPER DISTRIBUTION

Table 14: Influence of edge loss distribution on EGO dataset.

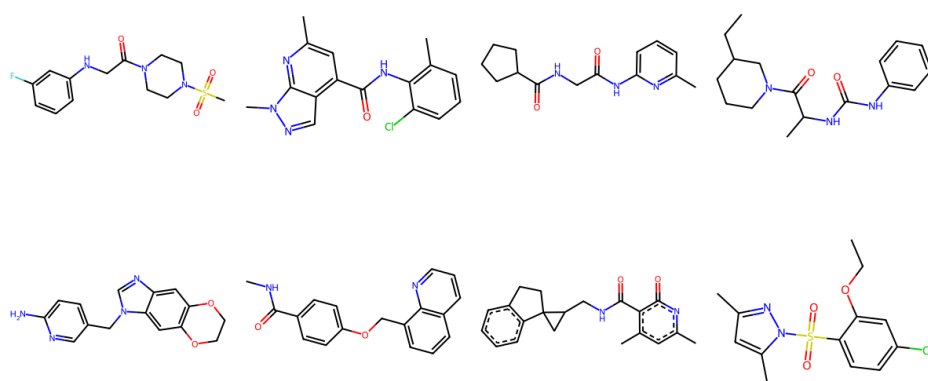
Loss based on	Deg ↓	Clus ↓	Orb ↓	Spec ↓	FID ↓	RBF MMD ↓
Comp graph	0.0021	0.0566	<b>0.0270</b>	0.0100	28.2	<b>0.0396</b>
Query graph	<b>0.0019±.00</b>	<b>0.0537±.00</b>	0.0299±.00	<b>0.0050±.00</b>	<b>16.1±12.9</b>	0.0483±.01

In order to emphasize the importance of preserving the edge distribution when computing losses, we conduct an experiment where we assess the performance of a model trained using all message-passing edges as opposed to solely using query edges. The former results in an increased emphasis on ‘existing’ edges during training compared to SparseDiff. Similarly, we use the Ego dataset for initial experiments. Table 14 shows that using edges of the message-passing graph  $G_m$  results in worse performance on most of the metrics, which indicates the importance of keeping a balanced edge distribution for loss calculation.

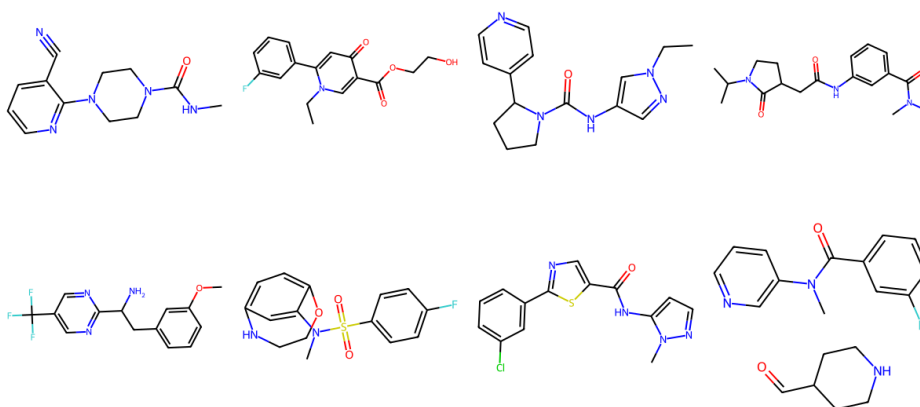
## E SOCIAL IMPACT

This paper aims to advance the field of graph generation. Our method enhances the training of larger graphs on limited GPU resources, enabling advancements in fields such as computational biology by allowing biologists to work with expansive protein graphs. It is also valuable in social network analysis and financial fraud detection by efficiently managing large-scale graphs, aiding in the understanding of complex patterns. While our work may have various societal implications as mentioned above, none are particularly harmful and thus do not require specific mention at this time.

## F VISUALIZATION

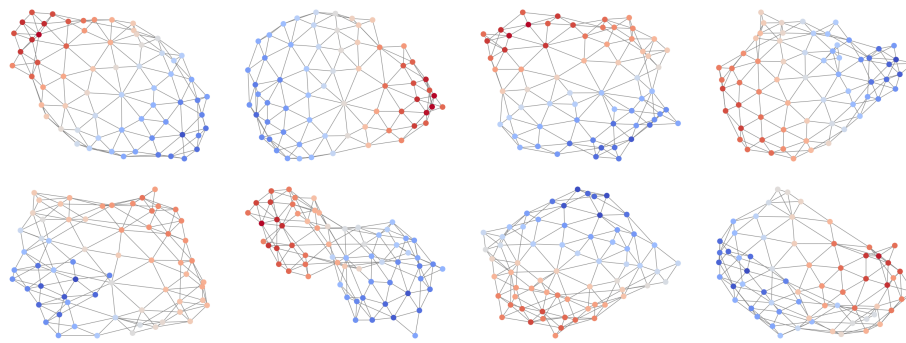


(a) Training graphs.

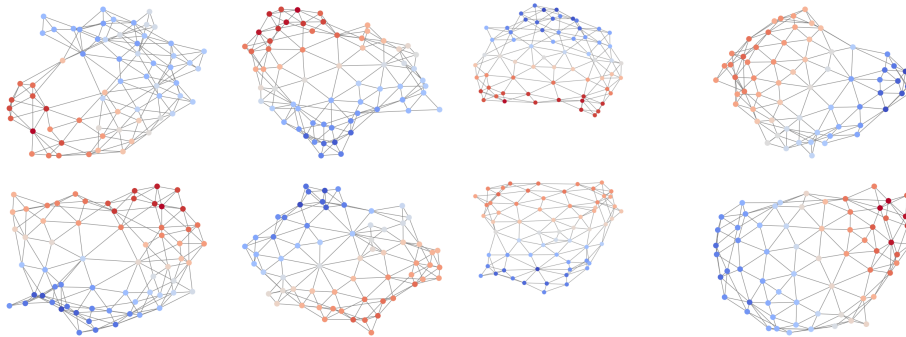


(b) Generated graphs.

Figure 9: Visualization for Moses dataset.

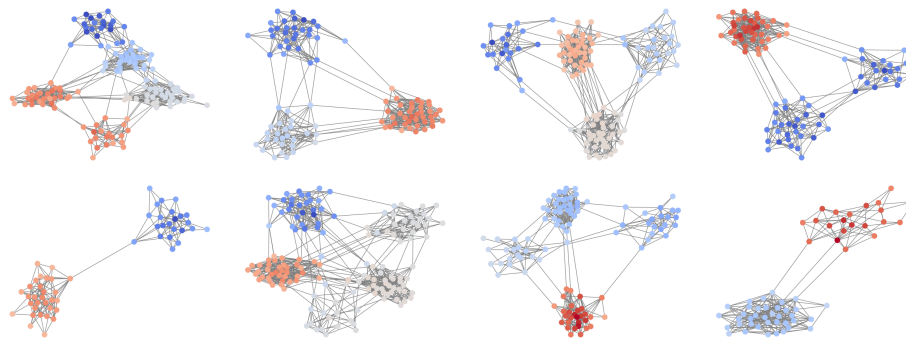


(a) Training graphs.

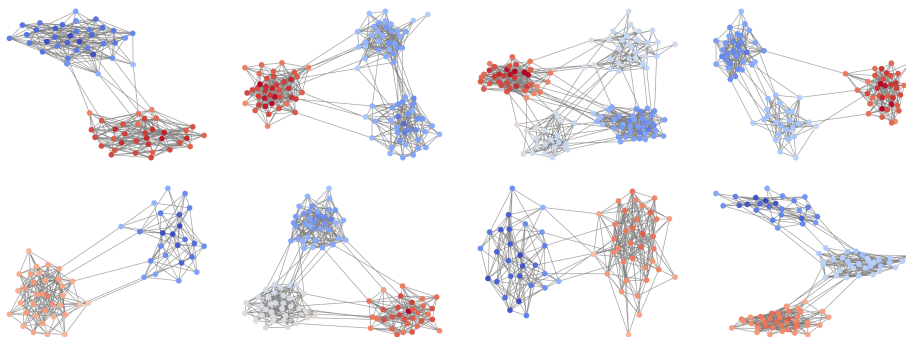


(b) Generated graphs.

Figure 10: Visualization for Planar dataset.

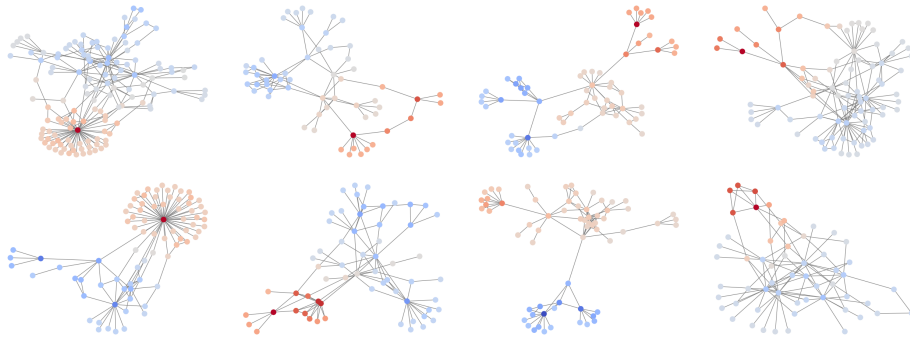


(a) Training graphs.

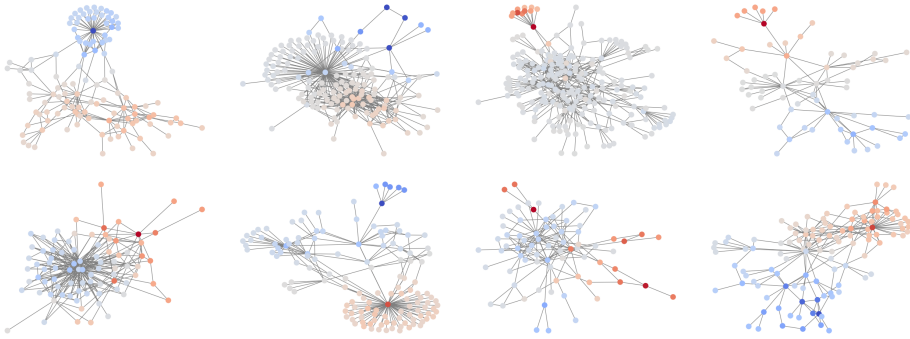


(b) Generated graphs.

Figure 11: Visualization for SBM dataset.

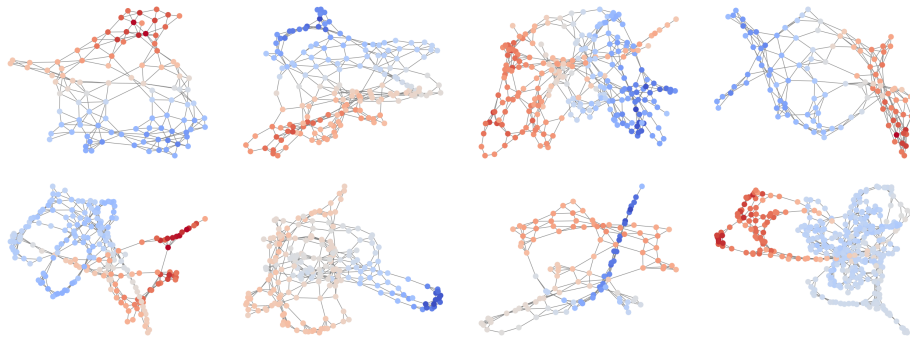


(a) Training graphs.

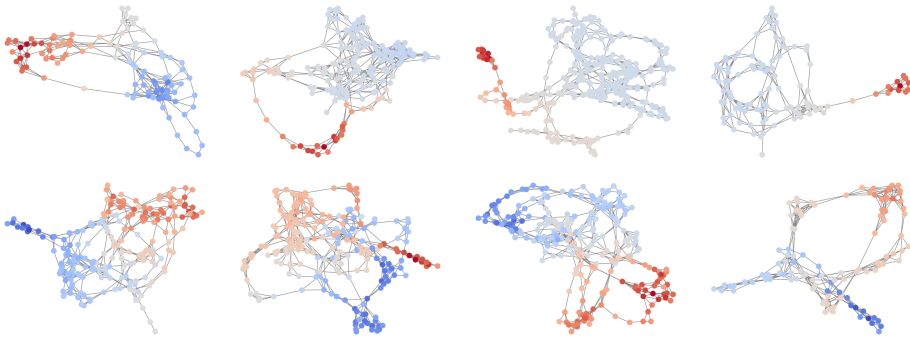


(b) Generated graphs.

Figure 12: Visualization for Ego dataset.



(a) Training graphs.



(b) Generated graphs.

Figure 13: Visualization for Protein dataset.